ELSEVIER

A Sensitivity Study of the SeaWiFS Atmospheric Correction Algorithm: Effects of Spectral Band Variations

*Menghua Wang**

With the success of launch and initial data processing of Sea-viewing Wide Field-of-view Sensor (SeaWiFS), there is a great interest in ocean color community to intercompare ocean color data between different ocean color sensors. It is well known that the atmospheric correction, which removes about **90%** *of sensor-measu red signals contributed from atmosphere in the visible, is the key procedure in ocean color imagery data processing. Therefore, it is useful to evaluate the SeaWiFS atmospheric correction algorithm applying to various ocean color sensors. The SeaWiFS atmospheric correction algorithm uses lookup tables which were generated with over -25,000 radiative transfer model runs for different aerosol optical and microphysical properties, solar and viewing geometries, and, in particular, at the eight SeaWiFS spectral bands. Since different ocean color sensors usually have different band spectral characterizations, it is rather difficult to apply the SeaWiFS atmospheric correction algorithm to other sensors if one needs to regenerate lookup tables at spectral bands different from SeaWiFS. In this article, we evaluate the accuracy of the SeaWiFS atmospheric correction algorithm for various ocean color sensors using the current SeaWiFS lookup tables. The focus in on the following satellite ocean color sensors: the Modular Optoelectronic Scanner (MOS), the Ocean Color and Temperature Sensor (OCTS), and the Polarization and Directionality of the Earth's Reflectances (POLDER). These sensor-s have a slightly different spectral bands compared with the SeaWiFS. It was found that, with an appropriate calculation of the Rayleigh scattering contributions at each sensor's spectral band and a simple modification in computing the diffuse transmittance of the ocean-atmosphere system, the SeaWiFS atmospheric correction applied to other sensors is as accurate as for SeaWiFS for the solar zenith angles* $\theta_0 \leq 60°$. *©Elsevier Science Inc., 1999*

INTRODUCTION

In the ocean color remote sensing, $<10\%$ of the sensor-measured radiance in the visible at satellite altitude is from the ocean near-surface water. This part of signals carries information concerning the concentration of phytoplankton which constitutes the first link in the marine food chain. Therefore, in the remote retrieval of the ocean near-surface properties, it is crucial to accurately remove the atmospheric effects from the sensor-measured radiance. This process is often termed as *atmospheric correction.* The atmospheric correction algorithm for Sea-viewing Wide Field-of-view Sensor (SeaWiFS) (Hooker et al., 1992) was developed by Gordon and Wang (1994a). The algorithm uses the SeaWiFS two near-infrared (NIR) bands (765 nm and 865 nm), where the ocean can usually be taken as a black surface, to estimate the atmospheric effect and extrapolate it into the visible. The Gordon and Wang algorithm is capable of retrieving the ocean nea-surface signals with an error $\leq 5\%$ at the blue, which meets the SeaWiFS goal. Implementation of the SeaWiFS atmospheric correction algorithm uses lookup tables which were generated with over -25,000 radiative transfer model runs for different aerosol optical and microphysical properties, solar and viewing geometries, and, in particular, at the eight SeaWiFS spectral bands.

Note that it is almost impossible to achieve the SeaWiFS goal purely through the prelaunch sensor radiometric calibration in the laboratory. For an uncertainty of 5% in the retrieved ocean near-surface signals at the

* University of Maryland Baltimore County, NASA Goddard Space Flight Center, Greenbelt

Address correspondence to M. Wang, NASA/GSFC, Code 970.2, Greenbelt, MD 20771. E-mail: wang@simbios.gsfc.nasa.gov

Received 17 February 1998; revised 18 September 1998.

REMOTE SENS. ENVIRON. 67:348–359 (1999)

655 Avenue of the Americas, New York, NY 10010

0034-4257/99/$–see front matter
PI1 S0034-4257(98)00095-9

blue, it appeared that one would require an uncertainty of the sensor radiometric calibration within -0.5%. In a recent article, however, Gordon (1998) outlined a methodology and strategy for achieving the required accuracy with a postlaunch *vicarious* calibration, that is, calibration of the whole system: the sensor and algorithms. With the vicarious calibration, the sensor measurement uncertainties in the visible can be significantly reduced relative to the NIR bands using the ground in *situ* measurements of the ocean and atmosphere optical properties. In such a vicarious calibration procedure, a 5% sensor calibration error at the blue can be reduced to -0.5% (Gordon, 1998). This gives necessary sensor calibration accuracy in the visible to be able to retrieve the ocean color information with the required accuracy. A similar vicarious calibration procedure has been employed for the SeaWiFS using the *in situ* measurements in the waters off Hawaii.

With the successful launch of SeaWiFS on 1 August 1997, there is interest in the ocean color community in intercomparing ocean color data between different ocean color sensors. It would be particularly useful if one could apply the SeaWiFS atmospheric correction to other sensors. The following ocean color sensors were launched in recent years and their sensor spectral characterizations are comparable with that of the SeaWiFS. They are Germany's Modular Optoelectronic Scanner (MOS) (Zimmermann and Neumann, 1997), Japan's Ocean Color and Temperature Sensor (OCTS) (Tanii et al., 1991), and France's Polarization and Directionality of the Earth's Reflectances (POLDER) (Deschamps et al., 1994). Also, a complicated and comprehensive satellite sensor, the Moderate Resolution Imaging Spectroradiometer (MODIS) (Salomonson et al., 1989), which has 36 spectral channels for remote sensing of the Earth's atmosphere, land, and ocean, is scheduled to be launched in 1999. To be flown on the same platform as MODIS, the Multi-angle Imaging Spectroradiometer (MISR) (Diner et al., 1989), which consists of a set of nine cameras that view the Earth at nine different angles and in four spectral bands (443 nm, 555 nm, 670 nm, and 865 nm), is capable of accurately retrieving the atmospheric aerosol properties from measurement of the angular distribution of radiance exiting the atmosphere (Wang and Gordon, 1994a; 1995), and possible ocean color observations (Gordon, 1997). The POLDER has a similar multiangle viewing geometry as that of the MISR. The MOS was launched in the spring of 1996 on the Indian IRS-P3 satellite and is still in operation. Therefore, one can obtain match-up scenes with the SeaWiFS. Both OCTS and POLDER have about 8 months ocean color data from October 1996 to June 1997. Table 1 provides the MOS, OCTS, and POLDER band spectral characterizations compared with the SeaWiFS. Spectral bands which are close to the SeaWiFS spectral channels are listed in the Table 1. Table 1 shows that different sensors usually have a slightly different spectral band characterization. It is difficult to apply the SeaWiFS correction algorithm to other sensors if one needs to regenerate lookup tables at spectral bands which are different from SeaWiFS. In this article, we investigate the sensitivity of the SeaWiFS atmospheric correction algorithm to sensor's spectral band variations. We first briefly review the Gordon and Wang atmospheric correction algorithm and its implementation into the SeaWiFS ocean color imagery data processing system. Next, we investigate the sensitivity of the current SeaWiFS aerosol lookup tables with spectral band variations for various aerosol optical properties and different solar and viewing geometries. We then test the accuracy of the atmospheric correction algorithm with various sensor's spectral band configurations for various cases using the current SeaWiFS aerosol lookup tables. Finally, we evaluate the accuracy in computing the diffuse transmittance of the ocean-atmosphere system with the spectral band variations and provide a formula to accurately account for the effects of slight band shift. Therefore, the SeaWiFS diffuse transmittance tables can still be used in the atmospheric correction for other ocean color sensors. In the Appendix, we provide some required parameters in the atmospheric correction for the MOS, OCTS, and POLDER compared with the SeaWiFS.

Table 1. The Sensor Spectral Band Characterization of SeaWiFS Compared with MOS, OCTS, and POLDER[a]

SeaWiFS Band Center (*nm*)	*MOS* Band Center (*nm*)	*OCTS* Band Center (*nm*)	*POLDER* Band Center (*nm*)
412	408	412	—
443	443	443	443
490	485	490	490
510	520	520	
555	570	565	565
670	685	670	670[b]
765	750	765	765
865	868	865	865[b]

[a] For other ocean color sensors. bands which are close to the SeaWiFS spectral bands are listed.
[b] Polarized channel.

THE SeaWiFS ATMOSPHERIC CORRECTION ALGORITHM

By defining the reflectance $\rho = \pi L / F_0 \cos\theta_0$, where L is the radiance in the given viewing direction, F_0 is the extraterrestrial solar irradiance, and θ_0 is the solar zenith angle, the total upward reflectance at the top of the ocean–atmosphere system, measured at a wavelength λ, can be written as

$$\rho_t(\lambda) = \rho_r(\lambda) + \rho_a(\lambda) + \rho_{ra}(\lambda) + t(\lambda)\rho_{wc}(\lambda) + t(\lambda)\rho_w(\lambda), \quad (1)$$

where $\rho_r(\lambda)$ is the reflectance resulting from multiple scat-

tering by air molecules (Rayleigh scattering) in the absence of aerosols, $\rho_a(\lambda)$ is the reflectance resulting from multiple scattering by aerosols in the absence of the air, $\rho_{ra}(\lambda)$ is multiple interaction term between molecules and aerosols (Deschamps et al., 1983), $\rho_{wc}(\lambda)$ is the reflectance at the sea surface that arises from sunlight and skylight reflecting from whitecaps on the surface (Gordon and Wang, 1994b), and $\rho_w(\lambda)$ is the water-leaving reflectance which is desired quantity in the ocean color remote sensing. The $t(\lambda)$ is the diffuse transmittance which accounts the effects of propagating water-leaving and whitecap reflectances from the sea surface to the top of the atmosphere (TOA). In the above equation, the surface sun glitter term has been ignored. The goal of the atmospheric correction is to retrieve the water-leaving reflectance $\rho_w(\lambda)$ accurately from the spectral measurements of reflectance $\rho_t(\lambda)$ at the satellite altitude. To relate the derived water-leaving reflectance to the ocean inherent optical properties (IOP), the atmospheric effects on the water-leaving reflectance $\rho_w(\lambda)$ must be removed. The normalized water-leaving radiance $[L_w(\lambda)]_N$ can be defined from Gordon and Clark (1981),

$$[L_w(\lambda)]_N = L_w(\lambda)/\cos\theta_0\, t(\lambda,\theta_0), \tag{2}$$

where $L_w(\lambda)$ is the water-leaving radiance and $t(\lambda,\theta_0)$ is the atmospheric diffuse transmittance in the solar direction with the solar zenith angle of θ_0. With the *in situ* measurements, one can estimate the atmospheric diffuse transmittance $t(\lambda,\theta_0)$ by measuring the downward irradiance $E_d(\lambda,\theta_0)$ just above the ocean surface. It can be shown that (Yang and Gordon, 1997) they are related as in Eq. (3):

$$E_d(\lambda,\theta_0) = F_0(\lambda)\cos\theta_0\, t(\lambda,\theta_0). \tag{3}$$

Therefore, the normalized water-leaving radiance in Eq. (2) can be rewritten as in Eq. (4):

$$[L_w(\lambda)]_N = F_0(\lambda)L_w(\lambda)/E_d(\lambda,\theta_0). \tag{4}$$

Both $L_w(\lambda)$ and $E_d(\lambda,\theta_0)$ can be obtained from the ground *in situ* measurements at the sea. The normalized water-leaving reflectance $[\rho_w(\lambda)]_N$ can be therefore defined through Eq. (2) as in Eq. (5):

$$[\rho_w(\lambda)]_N = \frac{\pi}{F_0(\lambda)}[L_w(\lambda)]_N \equiv \rho_w(\lambda)/t(\lambda,\theta_0). \tag{5}$$

Usually, the value of two-band ratio of $[\rho_w(\lambda)]_N$ (or $[L_w(\lambda)]_N$) in the visible can be used to infer the ocean near-surface optical properties (Gordon et al., 1988; Morel, 1988). Since 90% or more of signal measured at satellite altitude is contributed by the atmosphere and ocean surface [the first four terms in Eq. (1)], accurately removing these effects is considered to be a key to the success of any ocean color remote sensing experiment.

The Gordon and Wang atmospheric correction algorithm uses the SeaWiFS two NIR bands centered at 765 nm and 865 nm to estimate the atmospheric effects and extrapolate these into the visible range. The water-leaving reflectance $\rho_w(\lambda)$ at the two SeaWiFS NIR bands is usually negligible because of strong water absorption. Therefore, the radiances measured at these two NIR bands are essentially the contributions from atmosphere. Unlike Rayleigh scattering, which can be computed accurately, the aerosol scattering is highly variable, and the effects of the $\rho_a(\lambda)+\rho_{ra}(\lambda)$ in Eq. (1) on the imagery cannot be predicted *a* priori. Therefore, the difficulty of the atmospheric correction is in the process to accurately estimate the contributions from the multiple scattering of aerosols and the Rayleigh-aerosol interactions. Equation (1) can be rewritten as

$$\rho_t(\lambda) - \rho_r(\lambda) - t(\lambda)\rho_{wc}(\lambda) - t(\lambda)\rho_w(\lambda) = \rho_a(\lambda) + \rho_{ra}(\lambda). \tag{6}$$

Now, the left-hand side of Eq. (6) can be calculated from the sensor-measured radiance $\rho_t(\lambda)$, the computed Rayleigh scattering radiance $\rho_r(\lambda)$, and the estimated whitecap contributions at the SeaWiFS two NIR bands ($\rho_w=0$). These give the $\rho_a(\lambda)+\rho_{ra}(\lambda)$ values at these two NIR wavelengths. By using a set of candidate aerosol models, effects of the spectral variation of the $\rho_a(\lambda)+\rho_{ra}(\lambda)$ at the two NIR bands is then extrapolated into the visible, and water-leaving reflectance $\rho_w(\lambda)$ is retrieved there (Gordon and Wang, 1994a). The extrapolation was achieved through a process of aerosol model selection from evaluation of the atmospheric correction parameter, $\varepsilon(\lambda_i,\lambda_j)$, defined as (Gordon and Wang, 1994a; Wang and Gordon, 1994b)

$$\varepsilon(\lambda_i,\lambda_j) = \rho_{as}(\lambda_i)/\rho_{as}(\lambda_j),$$

where $\rho_{as}(\lambda_i)$ is the single scattering aerosol reflectance at a wavelength λ_i. The λ_j is usually at the longer NIR band, i.e., 865 nm. The value of $\varepsilon(\lambda_i,\lambda_j)$ characterizes the spectral variation of aerosol properties. As discussed by Wang and Gordon (1994b), the value of $\log_e[\varepsilon(\lambda_i,\lambda_j)]$ can be linearly related to λ_i. Therefore, the $\varepsilon(\lambda_i,\lambda_j)$ value can be accurately estimated for a slight wavelength shift. The SeaWiFS atmospheric correction algorithm is capable of retrieving $\rho_w(\lambda)$ at 443 nm with an error <0.001–0.002 for non- and weakly-absorbing aerosols, which usually is the case for region of open ocean where aerosols are generally generated locally. Although the open ocean covers the most ocean waters on the Earth, there are strong interests in the coastal area. For the coastal regions, however, there are some difficulties in correcting the atmospheric effects accurately. This is because not only the coastal regions are usually the case 2 water in which the water-leaving reflectance at the NIR bands are often not negligible but also the aerosols off the continents are likely absorbing. For these of the strongly absorbing aerosols, Gordon (1997) concluded from sensitivity studies that a set of realistic aerosol models with the representative of aerosol absorbing characteristics is necessary to be used in the aerosol lookup tables. This underscores importance of building an aerosol climatology

Table 2. Twelve Aerosol Models Used in Generating the SeaWiFS Lookup Tables

Model No.	*Aerosol Model*	*Relative Humidity (%)*
1–4	Maritime	50, 70, 90, and 99
5–8	Coastal	50, 70, 90, and 99
Y-12	Tropospheric	50, 70, 90, and 99

database to provide realistic aerosol models in the coastal regions.

The implementation of the Gordon and Wang algorithm into the SeaWiFS imagery data processing system was achieved through the use of lookup tables based on a large number (-25,000) of radiative transfer simulations that use the 12 aerosol models developed by Shettle and Fenn (1979). Table 2 shows the 12 aerosol models used in generating the SeaWiFS lookup tables. The main lookup tables contain information of the $\rho_a(\lambda) + \rho_{ra}(\lambda)$ values for different aerosol optical properties (12 aerosol models with various optical thicknesses) and various solar and viewing geometries at the eight SeaWiFS spectral bands. The other two tables, which are much smaller in data size, are, at the SeaWiFS spectral bands, for the Rayleigh scattering $\rho_r(\lambda)$ and the diffuse transmittance of the ocean-atmosphere system $t(\lambda)$. Since generating lookup tables for the $\rho_a(\lambda)+\rho_{ra}(\lambda)$ values involves a large number of radiative transfer simulations, it is rather difficult to implement the SeaWiFS atmospheric correction for other ocean color sensors if one needs to regenerate these tables at spectral bands which are different from that of SeaWiFS.

SENSITIVITY OF THE $\rho_a(\lambda)+\rho_{ra}(\lambda)$ WITH SPECTRAL BAND VARIATIONS

As shown in the Table 1, the most significant difference of spectral bands between the SeaWiFS and other ocean color sensors (MOS, OCTS, and POLDER) are the SeaWiFS Bands 4, 5, and 7. Table 3 shows their differences. Note that for a slight change of a spectral band, in terms of value of the $\rho_a(\lambda)+\rho_{ra}(\lambda)$, the main difference is from term $\rho_{ra}(\lambda)$ which is the term for Rayleigh-aerosol multiple interactions. Therefore, it is expected that with increasing wavelength (decreasing Rayleigh optical thickness), the effects of spectral band variation will be decreasing. Based on this, the MOS Band 6 was not listed in Table 3. However, it is necessary to investigate effects of variation at SeaWiFS Band 7 on the corrections at the visible since it is one of the two NIR bands used in the atmospheric corrections. Tables 1 and 3 show that, in the sensor spectral band characterization, the MOS is the most significantly different from the SeaWiFS.

Table 3. Spectral Band Difference between SeaWiFS and Other Sensors (MOS, OCTS, and POLDER) in the Selected SeaWiFS Channels

SeaWiFS Band No.	*MOS* $\Delta\lambda$ *(nm)*	*OCTS* $\Delta\lambda$ *(nm)*	*POLDER* $\Delta\lambda$ *(nm)*
4	10	10	—
5	15	10	10
7	-1 s	0	0

To understand the sensitivity of the spectral band variations in the generated p,(L) $+\rho_{ra}(\lambda)$ lookup tables, we have used the successive order of scattering code (Gordon and Wang, 1992) to compute reflectance $\rho_t(\lambda)$ of a two-layer atmosphere with the Rayleigh scattering above the aerosols bounded by a flat Fresnel-reflecting ocean for various aerosol models, aerosol optical thicknesses, and different solar and viewing geometries. We define λ_i and λ_i', respectively, as the SeaWiFS and other sensors (e.g., MOS) spectral wavelength at the band number i, where λ_i' is a slight shift from λ_i. The $\rho_t(\lambda_i')$ was first computed at the MOS wavelengths $\lambda_i'=520$ nm and 570 nm. The $\rho_t(\lambda_i')$ was considered as the MOS measured reflectance at the TOA. Next, the Rayleigh scattering $\rho_r(\lambda_i')$ was calculated at the wavelengths 520 nm and 570 nm. The $\rho_a(\lambda_i')+\rho_{ra}(\lambda_i')$ was then computed as in Eq. (6) by assuming that both $\rho_{wc}(\lambda_i')$ and $\rho_w(\lambda_i')=0$. The $\rho_a(\lambda_i')+\rho_{ra}(\lambda_i')$ at $\lambda_i'=520$ nm and 570 nm were taken as the true values for the MOS. Finally, taking the $\rho_a(\lambda_i)+\rho_{ra}(\lambda_i)$ from the SeaWiFS lookup tables, for example, at $\lambda_i=510$ nm and 555 nm, the error

$$\Delta(\lambda_i, \lambda_i')=[\rho_a(\lambda_i)+\rho_{ra}(\lambda_i)]-[\rho_a(\lambda_i')+\rho_{ra}(\lambda_i')]$$

for the MOS (OCTS) bands using the SeaWiFS lookup tables can be computed.

Figures la-d and 2a–d give examples of error $\Delta(\lambda_i, \lambda_i')$ (%) for the wavelengths $\lambda_i'=520$ and 570 nm using the SeaWiFS lookup tables at bands $\lambda_i=510$ nm and 555 nm for aerosol models Maritime with the relative humidity (RH) of 99% and Tropospheric with RH of 50% for various aerosol optical thicknesses as well as different solar and viewing geometries. Hereafter we denote M and T, respectively, for Maritime and Tropospheric aerosol models followed by a RH value, i.e., M99 stands for Maritime with RH=99%. In the 12 aerosol models used in the SeaWiFS lookup tables, M99 and T50 are usually the two extreme cases (the lowest and the highest) in the P M $+\rho_{ra}(\lambda_i)$ with changes of aerosol optical properties (Gordon and Wang, 1994a). Figures la-d are for the cases of $\lambda_i=510$ nm and $\lambda_i'=520$ nm, whereas Figures 2a–d are for the cases of $\lambda_i=555$ nm and $\lambda_i'=570$ nm. Figures la, lc, 2a, and 2c are for the cases of viewing at the center ($\theta=$ 1.02") for solar zenith angles θ_0 of 10–80°, while Figures lb, 1d, 2b, and 2d are for the cases of viewing at the edge ($\theta=45.9°$) for θ_0 of O-80". They are all for an azimuthal angle of $\Delta\varphi=90°$ and aerosol optical thicknesses of 0.05, 0.2, 0.4, and 0.6. Figures la-d and 2a–d show that, for $\theta_0 \leq 60°$, errors in computing $\rho_a(\lambda_i')+\rho_{ra}(\lambda_i')$ for $\lambda_i'=520$ nm and 570 nm using the SeaWiFS lookup tables at $\lambda_i=510$ nm and 555 nm are

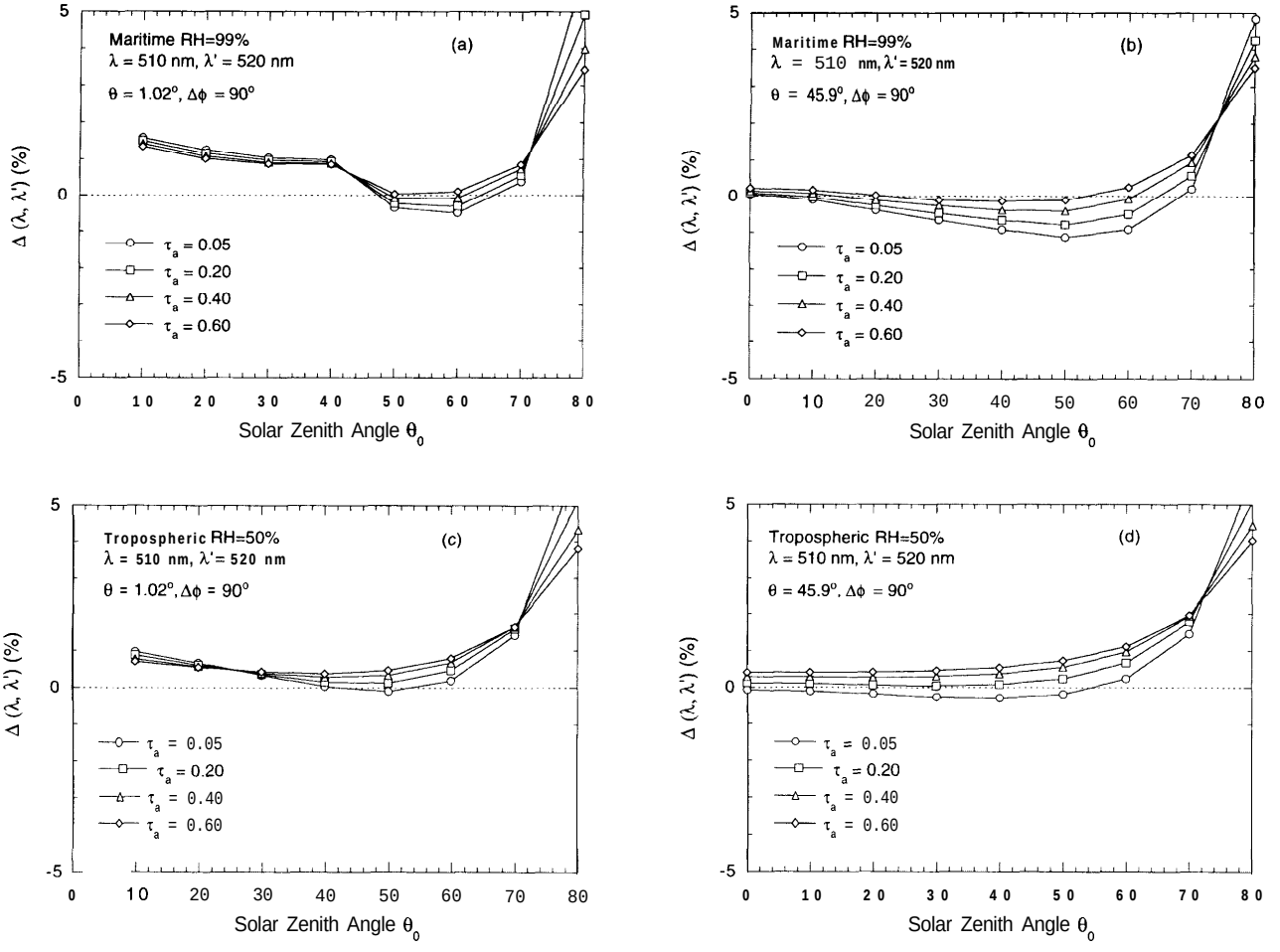

Figure 1. The errors $\Delta(\lambda,\lambda')$ (%) at λ=510 nm and λ'=520 nm for various aerosol optical thicknesses, solar zenith angles, and for aerosol model with viewing angles as: a) M90 and θ=1.02°; b) M90 and θ=45.9°; c) T50 and θ=1.02°; and d) T50 and θ=45.9°.

<1–2%. In the most cases, they are within 1%. Note that 1% of error in $\rho_a(\lambda)+\rho_{ra}(\lambda)$ corresponds to an absolute reflectance value of the order $\sim 10^{-5}$–10^{-4} depending on aerosol optical properties and solar and viewing geometries. It should point out that errors $\Delta(\lambda_i,\lambda_i')(\%)$ for the smaller aerosol optical thickness correspond to small difference error in the reflectance value, although they sometimes show the larger value in $\Delta(\lambda_i,\lambda_i')(\%)$ as in Figures lb and 2b.

PERFORMANCE OF THE SeaWiFS ATMOSPHERIC CORRECTION

To gain the sensitivity of the SeaWiFS atmospheric correction with spectral band variations, we have tested the SeaWiFS atmospheric correction for various spectral bands combinations with simulations. Following Gordon and Wang (1994a), we have applied the implemented SeaWiFS atmospheric correction algorithm to a series of simulations carried out using the Maritime and Tropospheric aerosol models with RH=80% (M80 and T80), that is, p,(A) was simulated with the M80 and T80 aerosol models at various spectral bands assuming both $\rho_{wc}(\lambda)$ and $\rho_w(\lambda)$=0. The $\rho_t(\lambda)$ was simulated as the sensor-measured upwelling reflectance at the TOA. The $\rho_r(\lambda)$ was computed exactly at a given spectral band. The $\rho_t(\lambda)$ value [with correct $\rho_r(\lambda)$] was inserted into the SeaWiFS atmospheric correction algorithm. The SeaWiFS $\rho_a(\lambda)+\rho_{ra}(\lambda)$ lookup tables were used for all computations reported in this article. The error in the retrieved water-leaving reflectance, $\Delta\rho(\lambda)\equiv t(\lambda)\Delta\rho_w(\lambda)$, was then computed. Figures 3-5 provide results of performance with the SeaWiFS atmospheric corrections for various spectral bands and different solar and viewing geometries. The aerosol optical thickness of τ_a=0.2 at 865 nm was used in all $\rho_t(\lambda)$ computations.

Figures 3a–d are results of $\Delta\rho(\lambda)$ at 443 nm for the cases of atmospheric correction using 765 nm and 865 nm (symbol 0) and 750 nm and 865 nm (symbol ❑). The first and the second case corresponds to, respectively, the SeaWiFS and the MOS spectral band characterization. Figures 3a and 3b are, respectively, for the M80

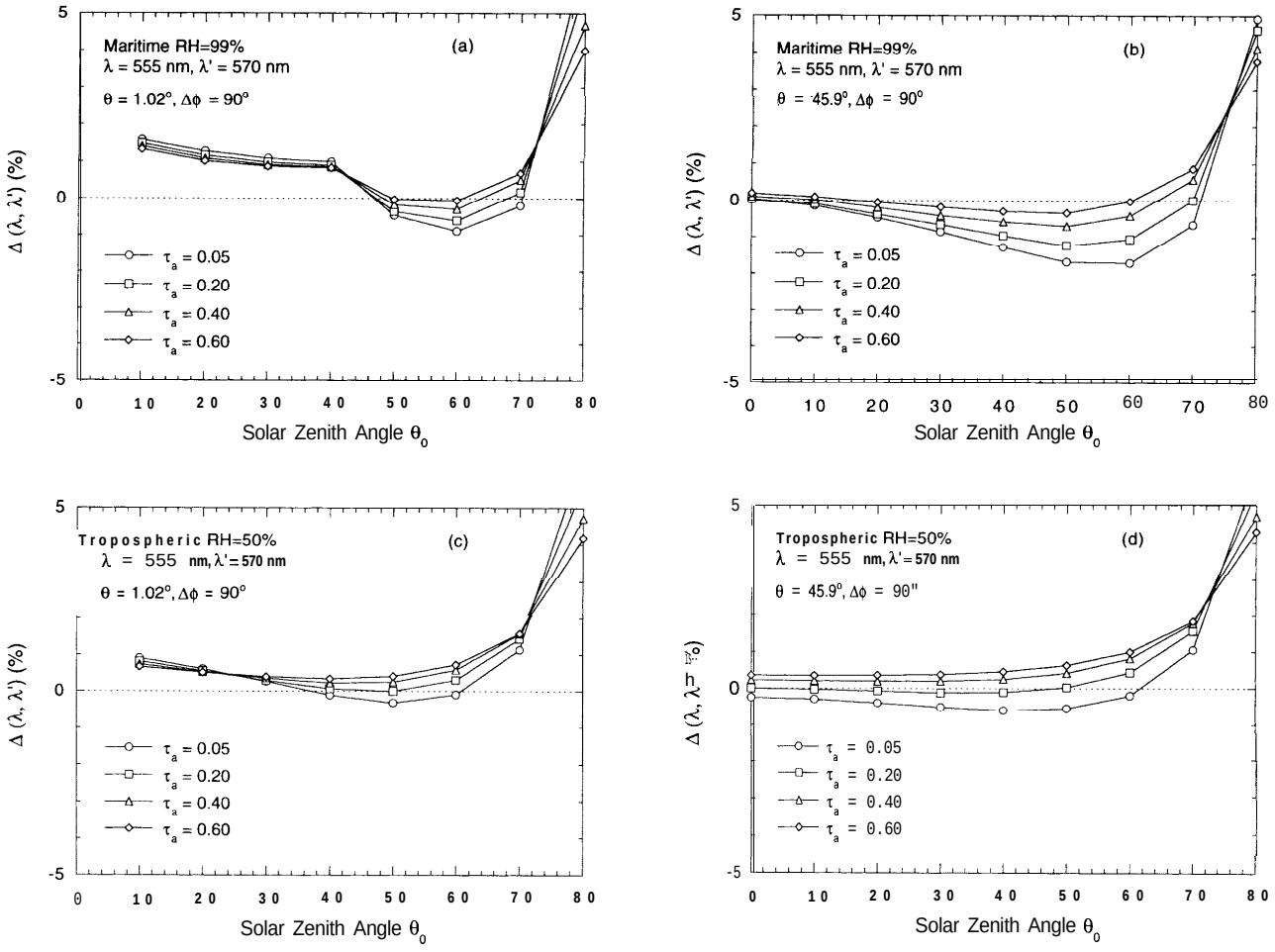

Figure 2. The errors $\Delta(\lambda,\lambda')$ (%) at λ=555 nm and λ'=570nm for various aerosol optical thicknesses, solar zenith angles, and for aerosol model and viewing angles as: a) M90 and θ=1.02°; b) M90 and θ=45.9°; c) T50 and θ=1.02°; and d) T50 and θ=45.9°.

aerosol model with viewing at the center (θ= 1.02") and edge (θ=45.9°), while Figures 3c and 3d are for the T80 aerosol cases. Figures 4a–d are for results of $\Delta\rho(\lambda)$ at the spectral bands **510** nm and 520 nm. There are three possible spectral bands combinations in the computations: i) Use 765 nm and **865** nm to correct atmospheric effects at 510 nm (SeaWiF) (symbol 0); ii) use 765 nm and 865 nm to correct atmospheric effects at 520 nm (OCTS) (symbol Cl); and iii) use 750 nm and 865 nm to correct atmospheric effects at 520 mn (MOS) (symbol △). Similarly, Figures 5a–d are for cases of $\Delta\rho(\lambda)$ at 555 nm and 570 nm, respectively. In all computations, the relative azimuthal angle $\Delta\varphi$ was taken to be 90".

Figures 3a–d show that the SeaWiFS Band 7 variation of 15 nm has almost no effects on accuracy in the retrieved water-leaving reflectance at the blue. Two curves have little difference for both the M80 and T80 aerosol models and for various solar and viewing geometries. They are all within error of **-0.001,** and in the most cases they are within **-0.0005.** On other hand, Figures 4 and 5 show that, for $\theta_0 \leqslant 60°$, the SeaWiFS atmospheric correction algorithm works quite well for the various spectral band variations. For large solar zenith angles ($\theta_0 > 60°$), however, error in the retrieved water-leaving reflectance increases dramatically in some cases (T80 aerosols). Except for cases of the T80 aerosol model with θ_0=60°, in which the error $\Delta\rho(\lambda)$ reaches about 0.001, the errors in retrieved water-leaving reflectance are all within ~0.0005 for $\theta_0 \leqslant 60°$. We conclude from these studies that, with appropriate computation of the Rayleigh scattering contribution at each sensor's spectral bands, the current SeaWiFS atmospheric correction, with the aerosol lookup tables $\rho_a(\lambda)+\rho_{ra}(\lambda)$, is as accurate for other sensors as for SeaWiFS for the solar zenith angles $\theta_0 \leqslant 60°$.

DIFFUSE TRANSMITTANCE COMPUTATIONS

Up to this point, we have discussed the sensitivity of the SeaWiFS atmospheric correction algorithm in retrieving the water-leaving reflectance at the TOA, that is, value

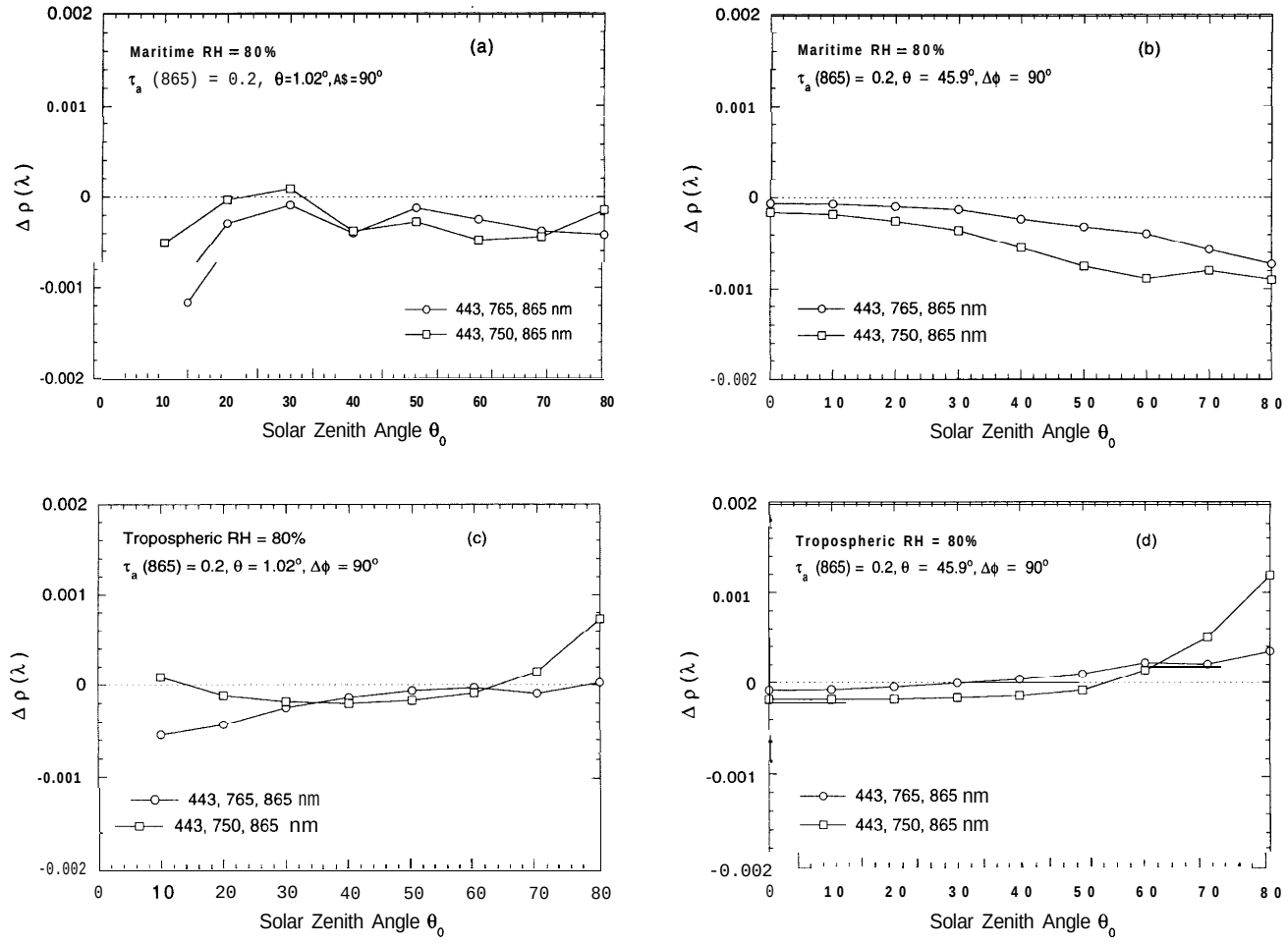

Figure 3. The errors $\Delta\rho(\lambda)$ in the retrieved $t(\lambda)\rho_w(\lambda)$ at 443 nm in comparison between the SeaWiFS and the MOS spectral configurations for various solar zenith angles and for aerosol model and viewing angle as: a) M80 and θ=1.02°; b) M80 and θ=45.9°; c) T80 and θ=1.02°; and d) T80 and θ=45.9°.

of $t(\lambda)\rho_w(\lambda)$. To recover the water-leaving reflectance just above the ocean surface $\rho_w(\lambda)$ from $t(\lambda)\rho_w(\lambda)$, however, one needs the atmosphere transmittance which propagates the water-leaving reflectance from the sea surface to the TOA. The diffuse transmittance of a Rayleigh-aerosol atmosphere can be approximated by (Gordon et al., 1983)

$$t(\lambda,\theta)=\exp[-(\tau_r(\lambda)/2+(1-\omega_a(\lambda)F_a(\lambda))\tau_a(\lambda))/\cos\theta]. \quad (7)$$

In Eq. (7) ω_a is the aerosol single scattering albedo and τ_r and τ_a are the optical thicknesses for air molecules and aerosols at a wavelength λ, respectively. The term $\omega_a F_a$ is the probability that, in a single scattering case, a photon will be scattered by aerosols through an angle of <90°. The values of ω_a, F_a, and τ_a depend on both wavelength and the aerosol model. Note that the transmittance for ozone, $t_{Oz}=\exp[-\tau_{Oz}/\cos\theta]$, where τ_{Oz} is the ozone optical thickness, is not included in the above equation. The ozone effect has been assumed to be taken into account in reflectance before go into the atmospheric correction. The diffuse transmittance values for SeaWiFS were tabulated from data of ~25,000 simulations using the exponential fitting as in Eq. (8):

$$t(\lambda_i,\theta)=A(\lambda_i,\theta)\exp[-B(\lambda_i,\theta)\tau_a(\lambda_i)], \quad (8)$$

where $A(\lambda_i,\theta)$ and $B(\lambda_i,\theta)$ are fitting coefficients for the eight SeaWiFS spectral bands, 12 aerosol models, and various solar and viewing geometries (Yang and Gordon, 1997). The $t(\lambda_i,\theta)$ values from the tables are very accurate with accuracy usually within 0.1%. Note that the $t(\lambda_i,\theta)$ values as well as the aerosol lookup tables, $\rho_a(\lambda_i)+\rho_{ra}(\lambda_i)$, were generated at the nominal center wavelengths of the SeaWiFS spectral bands. Table 4 gives the extraterrestrial solar irradiance from Neckel and Labs (1984) and the Rayleigh optical thickness values at wavelengths of the eighth SeaWiFS spectral band centers. As discussed in the Appendix, to account for sensor spectral variation within each band, the averaged Rayleigh optical thickness, which is weighted by sensor's band spectral response function (SRF) and the solar irradiance, has to be used in computing the diffuse transmittance. Therefore, even for the SeaWiFS, the band averaged transmittance values are different from those of the transmittance tables.

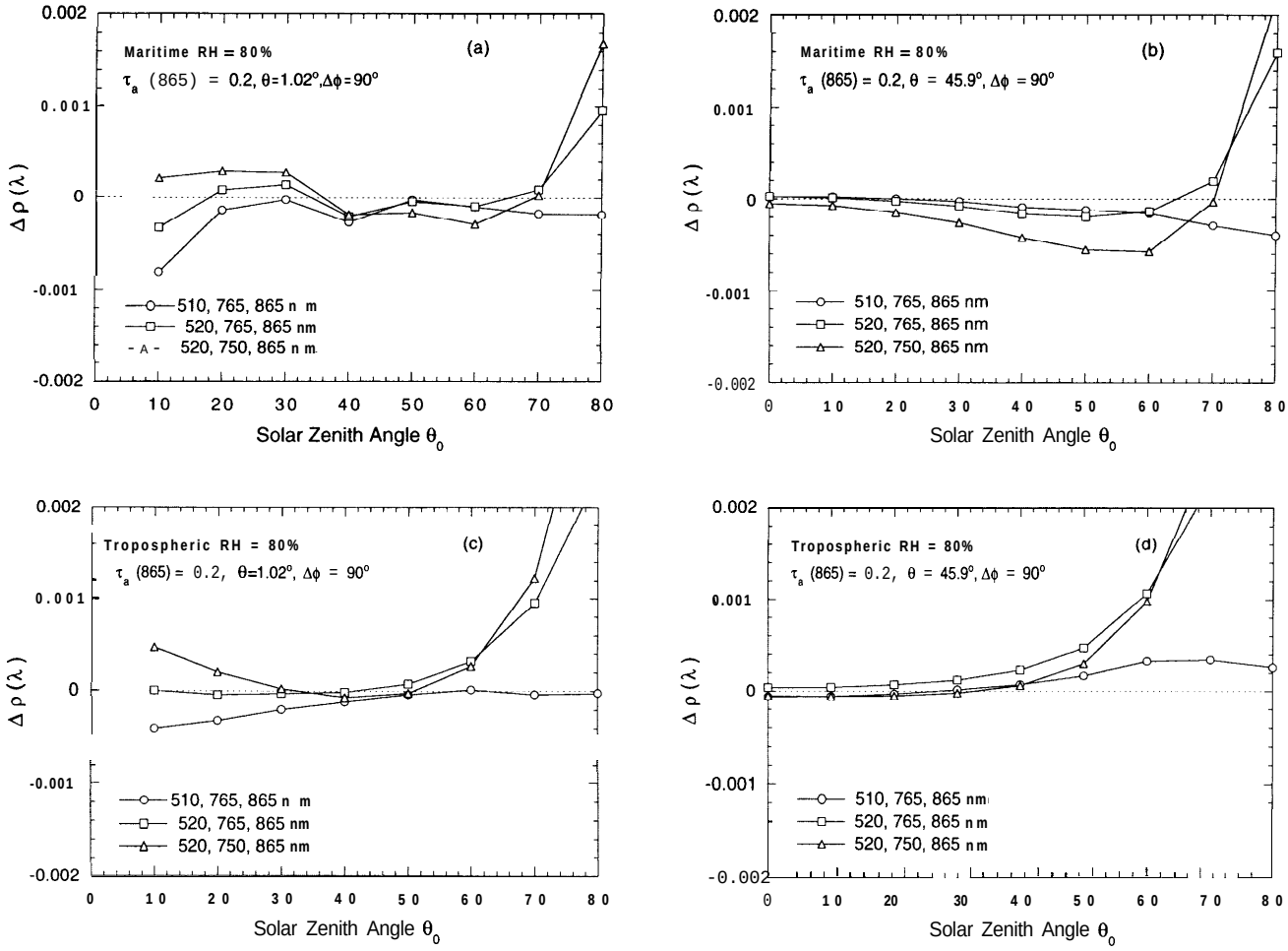

Figure 4. The errors $\Delta\rho(\lambda)$ in the retrieved $t(\lambda)\rho_w(\lambda)$ at 510 nm and 520 nm with various spectral configurations for various solar zenith angles and aerosol model and viewing angle as: a) M80 and $\theta=1.02°$; b) M80 and $\theta=45.9°$; c) T80 and $\theta=1.02°$; and d) T80 and $\theta=45.9°$.

We have studied the sensitivity of the diffuse transmittance with spectral band variations, and found that, directly using the SeaWiFS transmittance tables without any modifications for a slight change of wavelengths, the errors in diffuse transmittance are about 0.51.0%. In the study, the true values of the diffuse transmittance $t^{(m)}(\lambda_i',\theta)$ were computed by first solving the radiative transfer equation using the successive order of scattering method for a two-layer atmosphere bounded by a flat Fresnel-reflecting ocean at the wavelengths $\lambda_i'=520$ nm and 570 nm for a given aerosol model, aerosol optical thickness, and the sensor viewing angle. The $t^{(m)}(\lambda_i',\theta)$ was obtained using the reciprocity principle (Yang and Gordon, 1997), assuming that the angular distribution of the upwelling radiance beneath the sea surface is uniform. Assuming $t(\lambda_i',\theta)$ is an approximation of the true value $t^{(m)}(\lambda_i',\theta)$, the error

$$\Delta t(\lambda_i',\ \lambda_i,\ \theta)=t(\lambda_i',\ \theta)-t^{(m)}(\lambda_i',\ \theta)$$

was then computed. To improve the accuracy, we have tested in modifying diffuse transmittance computations in the following two ways:

$$t(\lambda_i',\theta)=t(\lambda_i,\theta)\exp[-(\tau_r(\lambda_i')-\tau_r(\lambda_i))/2\cos\theta] \qquad (9)$$

and

$$t(\lambda_i',\ \theta)=t(\lambda_i,\ \theta)\ \exp[-(\tau_r(\lambda_i')-\tau_r(\lambda_i))/2], \qquad (10)$$

where $t(\lambda_i,\theta)$ was taken from the SeaWiFS lookup tables at the SeaWiFS spectral band λ_i, while $t(\lambda_i',\theta)$ was computed for other sensors at spectral band λ_i'. Therefore, we test the accuracy of $t(\lambda_i',\theta)$ computation in three ways: i) directly using the SeaWiFS transmittance tables without any modifications; ii) modified as Eq. (9); and iii) modified as Eq. (10). Figures 6a and 6b provide examples of errors (%) in computing $t(\lambda_i',\theta)$ in three different ways for the wavelengths of 520 nm and 570 nm for aerosol models M99 and T50, aerosol optical thickness from 0.05 to 0.8, and the sensor viewing angles from 0" to 80". Figure 6a is for the MOS (OCTS) band at 520 nm, while Figure 6b is for the band at 570 nm. The circles (0) in these figures are for case i) that the diffuse transmittances for the MOS were simply from the

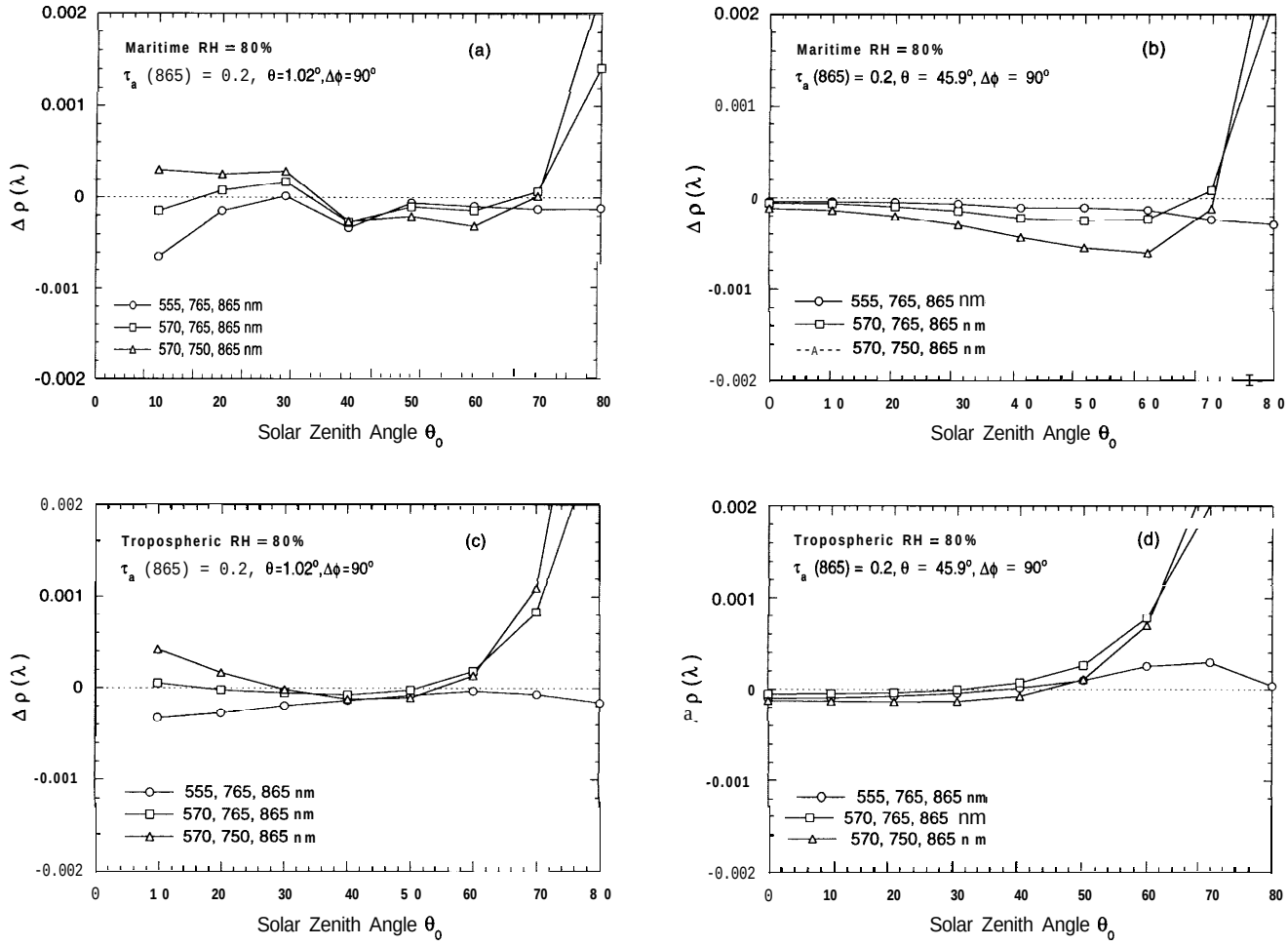

Figure 5. The errors $\Delta\rho(\lambda)$ in the retrieved $t(\lambda)\rho_u(\lambda)$ at 555 nm and 570 nm with various spectral configurations for various solar zenith angles and for aerosol model and viewing angle as: a) M80 and θ= 1.02"; b) M80 and θ=45.9°; c) T80 and θ=1.02°; and d) T80 and θ=45.9°.

SeaWiFS lookup tables without any modifications, that is, $t(\lambda_i', \theta)$=$t(\lambda_i, \theta)$. The errors $\Delta t(\lambda_i', \lambda_i, \theta)$ are about 0.5–1.0%, depending on sensor viewing angles. The other symbols in figures are for cases ii) and iii), where the diffuse transmittances were modified according to Eqs. (9) (symbols Cl) and (10) (symbols △) with $t(\lambda_i, \theta)$ values from the SeaWiFS transmittance tables. Note that, for a given viewing angle θ, values of $\Delta t(\lambda_i', \lambda_i, \theta)$ in Figure 6 were computed for the two aerosol models (M99 and T50) and eight aerosol optical thicknesses from the 0.05 to 0.8 total of 18 values. Figure 6 shows that both Eqs. (9) and (10) are very accurate in computing the diffuse transmittance for the viewing angles up to 60" for aerosol models M99 and T50 and aerosol optical thicknesses from 0.05 to 0.8. The *maximum* error in $t(\lambda_i', \theta)$ computation was about 0.3% for both cases for $\theta \leq 60°$. For viewing angles $\theta > 60°$, however, Eq. (9) gives larger errors since effects of $\tau_r/\cos\theta$ increase dramatically, whereas Eq. (10) is still quite accurate. We conclude that, using the SeaWiFS transmittance tables with modification as Eq. (10), the diffuse transmittance for other sensors, with slight spectral band variations, can be obtained within the accuracy of about 0.5% (usually within 0.1%).

Table 4. Values of the Solar Irradiance and the Rayleigh Optical Thickness at the Nominal Center Wavelength of the SeaWiFS Spectral Bands"

SeaWiFS Band No.	F_0 $[mW/(cm^2\ \mu m\ sr)]$	τ_r
1	180.80	0.3185
2	194.95	0.2361
3	198.85	0.1560
4	193.65	0.1324
5	190.25	0.0938
6	153.50	0.0436
7	122.40	0.0255
8	97.10	0.0155

[a] These Rayleigh optical thicknesses were used in generating $\rho_a(\lambda) + \rho_{rm}(\lambda)$ and the diffuse transmittance tables.

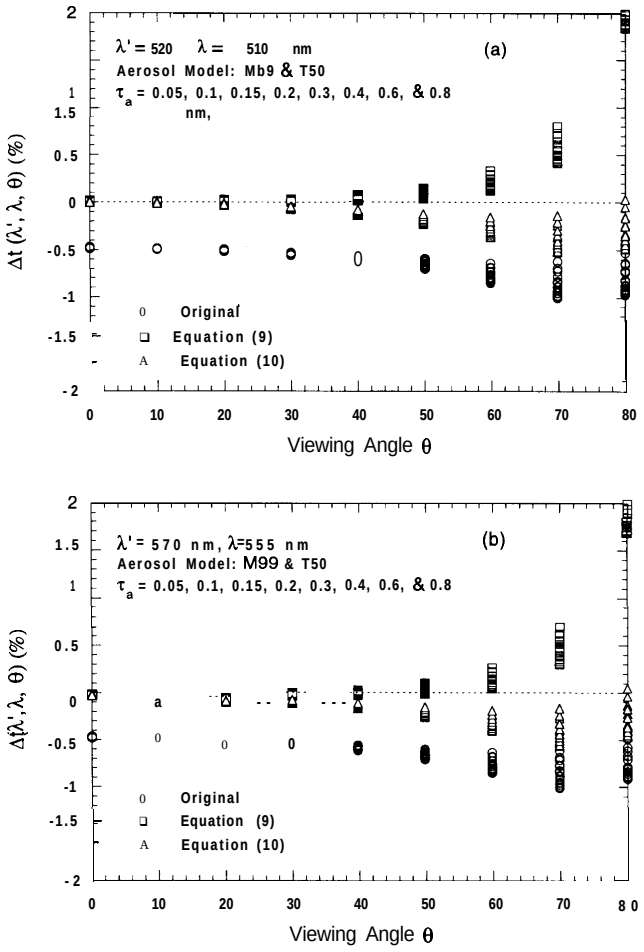

Figure 6. The errors $\Delta t(\lambda', \lambda, \theta)(\%)$ in computing $t(\lambda', \theta)$ in three different ways: i) data from SeaWiFS tables without any modifications, ii) modified as Eq.(9), and iii) modified as Eq. (10) for the aerosol models M99 and T50, aerosol optical thicknesses 0.05–0.8, and viewing angles θ from 0" to 80" for a) $\lambda'=520$ nm with the SeaWiFS data at $\lambda=510$ nm and b) $\lambda'=570$ nm with the SeaWiFS data at $\lambda=555$ nm.

CONCLUSIONS

We have studied the sensitivity of the current SeaWiFS atmospheric correction algorithm with variation of the spectral bands for various satellite ocean color sensors. Our goal is to assess the efficacy of the current SeaWiFS atmospheric correction algorithm with its lookup tables for the spectral band variation, so that it can be applied to various ocean color sensors, for example, MOS, OCTS, and POLDER. We found that, by accurately computing the Rayleigh scattering reflectance at the sensor's spectral bands, the current SeaWiFS $\rho_a(\lambda)+\rho_{ra}(\lambda)$ lookup tables are accurate within 1% for the most cases for various spectral band variations, aerosol optical properties, and different solar and viewing geometries. Furthermore, we have tested the accuracy of the SeaWiFS atmospheric correction in retrieval of the water-leaving reflectance at various spectral bands for different sensors using the current SeaWiFS $\rho_a(\lambda)+\rho_{ra}(\lambda)$ lookup tables. The results show that the algorithm works quite well for the various cases for the solar zenith angles $\theta_0 \leq 60°$. Finally, we have estimated the accuracy of the diffuse transmittance computation using the SeaWiFS transmittance tables for the various spectral bands in which there are a slight variations from the SeaWiFS bands. By a simple modification, the diffuse transmittance can be usually computed, using the SeaWiFS transmittance tables, within the accuracy of about 0.1%.

In summary, to apply the implemented SeaWiFS atmospheric correction algorithm to other ocean color sensors (e.g., MOS, OCTS, and POLDER), one needs to, according to sensor's spectral band characterizations, i) recompute the extraterrestrial solar u-radiances and ozone absorption coefficients, ii) regenerate the Rayleigh scattering reflectance tables, and iii) modify the diffuse transmittance tables with a simple formula. The retrieved water-leaving reflectance for other ocean color sensors using the SeaWiFS atmospheric correction package is as accurate as for SeaWiFS for the solar zenith angles $\theta_0 \leq 60°$.

Table 5. Values of the Averaged Solar Irradiance (F_{0}) for MOS, OCTS, and POLDER Compared with SeaWiFS"

	(F_0) [mW/(cm² μm sr)]			
Band No.	*SeaWiFS*	*MOS*	*OCTS*	*POLDER*
1	170.79	168.77	171.06	—
2	189.45	189.03	188.48	189.92
3	193.66	194.73	194.56	193.13
4	188.35	182.36	185.59	
5	185.33	18459	183.33	184.66
6	153.41	147.48	152.43	152.94"
7	122.24	127.26	122.39	123.04
8	98.82	96.65	98.48	98.60"

[a] $\langle F_0 \rangle$ was computed as weighted by the band spectral response function for a given sensor.
[b] Polarized channel.

APPENDIX: QUANTITIES NEEDED IN THE ATMOSPHERIC CORRECTIONS

Following Gordon (1995), we provide values of the sensor band averaged solar irradiance, Rayleigh optical thickness, and ozone absorption coefficient for MOS, OCTS, and POLDER compared with SeaWiFS. Since the lookup tables $\rho_a(\lambda)+\rho_{ra}(\lambda)$ are in reflectance units, the solar irradiance values are needed to convert the sensor-measured radiance to reflectance. To account for the sensor band spectral variations, one needs to use the averaged solar irradiance weighted by band spectral response function (SRF), that is, as in Eq. (11):

$$\langle F_0(\lambda) \rangle_j = \frac{\int F_0(\lambda) S_j(\lambda)\, d\lambda}{\int S_j(\lambda)\, d\lambda}, \qquad (11)$$

where $F_0(\lambda)$ is the extraterrestrial solar irradiance and

Table 6. Values of the Averaged Rayleigh Optical Thickness $\langle \tau_r \rangle$ for MOS, OCTS, and POLDER Compared with SeaWiFS"

	$\langle \tau_r \rangle$			
Band No.	*SeaWiFS*	*MOS*	*OCTS*	*POLDER*
1	0.3132	0.3322	0.3131	—
2	0.2336	0.235 1	0.2335	0.2326
3	0.1547	0.1640	0.1557	0.1535
4	0.1330	0.1220	0.1266	—
5	0.0947	0.084 1	0.0859	0.0876
6	0.0446	0.0399	0.0440	0.0436[b]
7	0.0256	0.0278	0.0256	0.0259
8	0.0169	0.0153	0.0158	0.0 159"

[a] (T,) was computed as weighted by the solar irradiance and the hand spectral response function for a given sensor.
[b] **Polarized** channel.

Table 7. Values of the Averaged Ozone Absorption Coefficient $\langle k_{Oz} \rangle$ for MOS, OCTS, and POLDER Compared with SeaWiFS"

	$\langle k_{Oz} \rangle$ (x 1 0^{-6}) (*Dobson* $^{-1}$)			
Band No.	*SeaWiFS*	*MOS*	*OCTS*	*POLDER*
1	1.03	0.76	1.53	
2	4.00	3.79	4.36	4.12
3	25.36	21.20	24.97	2.5.64
4	42.00	49.30	46.98	
5	93.38	123.48	111.17	111.63
6	46.85	33.95	47.35	45.54"
7	8.37	10.21	8.27	8.46
8	4.85	3.67	3.73	3.74"

[a] $\langle k_{Oz} \rangle$ was computed as weighted by the solar irratliance and the band spectral response function for a given sensor.
[b] Polarized channel.

$S_j(\lambda)$ is the SRF for the jth spectral band for a given sensor. Table 5 gives the averaged solar u-radiance values $\langle F_0 \rangle$ for SeaWiFS, MOS, OCTS, and POLDER. Table 6 provides the values of averaged Rayleigh optical thickness $\langle \tau_r \rangle$ needed in generating the Rayleigh scattering reflectances tables $\rho_r(\lambda)$ for various ocean color sensors. The $\langle \tau_r \rangle$ values were computed as weighted by the solar n-radiance and the sensor band SRF as in Eq. (12):

$$\langle \tau_r(\lambda) \rangle_j = \frac{\int \tau_r(\lambda) F_0(\lambda) S_j(\lambda)\, d\lambda}{\int F_0(\lambda) S_j(\lambda)\, d\lambda}. \qquad (12)$$

This $\langle \tau_r \rangle$ value should be used in generating the Rayleigh scattering tables as well as in computing the atmosphere diffuse transmittance. In a similar way, Table 7 gives the values of averaged ozone absorption coefficient $\langle k_{Oz} \rangle$ needed in calculating the ozone optical thickness for SeaWiFS, MOS, OCTS, and POLDER. The ozone absorption coefficient data $k_{Oz}(\lambda)$ was from Nicolet **(1981).** The ozone optical thickness $\langle \tau_{Oz} \rangle$ can be related to $\langle k_{Oz} \rangle$ through Eq. **(13):**

$$\langle \tau_{Oz}(\lambda) \rangle_j = \langle k_{Oz}(\lambda) \rangle_j (DU), \qquad \textbf{(13)}$$

where DU is the ozone concentration in milliatmosphere-centimeter (Dobson units). The two-way ozone transmittance is then given by Eq. **(14):**

$$t_{Oz}(\lambda, \theta, \theta_0) = \exp\left[-\langle \tau_{Oz}(\lambda) \rangle_j \left(\frac{1}{\cos \theta} + \frac{1}{\cos \theta_0} \right) \right], \qquad (14)$$

where θ_0 and θ are the solar and sensor zenith angles, respectively. In computing $\langle F_0 \rangle, \langle \tau_r \rangle$, and $\langle k_{Oz} \rangle$, the solar irradiance data $F_0(\lambda)$ are from Neckel and Labs (1984). In Tables 5-7, the band number is for the sensor bands listed as shown in Table 1, which is corresponding to the SeaWiFS spectral bands from 412 nm to 865 nm.

This research was supported by funding provided by the National Aeronautics and Space Administration under the Sensor Intercomparison and Merger for Biological and Interdisciplinary Oceanic Studies (SIMBIOS) project.

REFERENCES

Des&amps, P. Y., Herman, M., and Tanré, D. (1983), Modeling of the atmospheric effects and its application to the remote sensing of ocean color. *Appl. Opt.* 22:3751–3758.

Deschamps, P. Y., Bréon, F. M., Leroy, M., et al. (1994), The POLDER mission: instrument characteristics and scientific objectives. *IEEE Trans. Geosci. Remote Sens.* 32:598–615.

Diner, D. J., Bruegge, C. J., Martonchick, J. V., et al. (1989), MISR: a multi-angle Imaging SpectroRadiometer for geophysical and climatological research from EOS. *ZEEE Trans. Geosci. Remote Sens.* 27:200–214.

Gordon, H. R. (1995), Remote sensing of ocean color: a methodology for dealing with broad spectral bands and significant out-of-band responses. *Appl. Opt.* 34:8363–8374.

Gordon, H. R. (1997), Atmospheric correction of ocean color imagery in the Earth Observing System era. *J. Geophys. Res.* 102:17,081–17,106.

Gordon, H. R. (1998), In-orbit calibration strategy for ocean color sensors. *Remote Sens. Environ.* 63:265–278.

Gordon, H. R., and Clark, D. K. (1981), Clear water radiances for atmospheric correction of coastal zone color scanner imagery. *Appl. Opt.* 20:4175–4180.

Gordon, H. R., and Wang, M. (1992), Surface roughness considerations for atmospheric correction of ocean color sensors. 1: The Rayleigh scattering component. *Appl. Opt.* 31:4247–4260.

Gordon, H. R., and Wang, M. (1994a), Retrieval of water-leaving radiance and aerosol optical thickness over the oceans with SeaWiFS: a preliminary algorithm. *Appl. Opt.* 33:443–452.

Gordon, H. R., and Wang, M. (1994b), Influence of oceanic whitecaps on atmospheric correction of ocean-color sensor. *Appl. Opt.* 33:7754–7763.

Gordon, H. R., Brown, 0. B., Evans, R. H., et al. (1988), A semianalytic radiance model of ocean color. *J. Geophys. Res. 93:* 10,909–10,924.

Gordon, H. R., Clark, D. K., Brown, J. W., Brown, 0. B., Evans, R. H., and Broenkow, W. W. (1983), Phytoplankton pigment concentrations in the Middle Atlantic Bight: comparison of ship determinations and CZCS estimates. *Appl. Opt.* 22:20–36.

Hooker, S. B., Esaias, W. E., Feldman, G. C., Gregg, W. W., and McClain, C. R. (1992), An overview of SeaWiFS and

ocean color, NASA Goddard Space Flight Center, Greenbelt, MD.

Morel, A. (1988), Optical modeling of the upper ocean in relation to its biogenous matter content (case 1 waters). *J. Geophys. Res. 93:* 10,749–10,768.

Neckel, H., and Labs, D. (1984), The solar radiation between 3300 and 12500 Å. Solar *Phys.* 90:205–258.

Nicolet, M. (1981), The solar spectral irradiance and its action in the atmospheric photodissociation processes. *Planet. Space Sci.* 29:951–974.

Salomonson, V.V., Barnes, W. L., Maymon, P. W., Montgomery, H. E., and Ostrow, H. (1989), MODIS: advanced facility instrument for studies of the Earth *as a* system. *IEEE Trans. Geosci. Remote Sens. 27:* 145-152.

Shettle, E. P., and Fenn, R. W. (1979), Models for the aerosols of the lower atmosphere and the effects of humidity variations on their optical properties, U.S. Air Force Geophysics Laboratory, Hanscom Air Force Base, MA.

Tanii, J., Machida, T., Ayada, H., et al. (1991), Ocean color and temperature scanner (OCTS) for ADEOS. *SPZE* 1490: 200-206.

Wang, M., and Gordon, H. R. (1994a), Estimating aerosol optical properties over the oceans with the Multiangle Imaging SpectroRadiometer: some preliminary studies. *Appl. Opt.* 33:4042–4057.

Wang, M., and Gordon, H. R. (1994b), A simple, moderately accurate, atmospheric correction algorithm for SeaWiFS. *Remote Sens. Environ.* 50:231–239.

Wang, M., and Gordon, H. R. (1995), Estimation of aerosol columnar size distribution and optical thickness from the angular distribution of radiance exiting the atmosphere: simulations. *Appl. Opt.* 34:6989–7001.

Yang, H., and Gordon, H. R. (1997), Remote sensing of ocean color: assessment of water-leaving radiance bidirectional effects on atmospheric diffuse transmittance. *Appl. Opt. 36: 7887-7897.*

Zimmermann, G., and Neumann, A. (1997), The Spaceborne Imaging Spectrometer MOS for ocean remote sensing. In *Proceedings of the 1st International Workshop on MOS-IRS and Ocean Color,* DLR, Institute of Space Sensor Technology, Berlin, pp. 1-9.